Phonon Spectrum of Scandium Metal by Inelastic Scattering of Neutrons†

N. Wakabayashi,* S. K. Sinha, and F. H. Spedding
Institute for Atomic Research and Department of Physics, Iowa State University, Ames, Iowa 50010
(Received 29 March 1971)

The phonon dispersion relations along the principal symmetry axes of the hexagonal close-packed metal scandium have been measured at room temperature by means of inelastic neutron scattering. The results have been analyzed in terms of a sixth-neighbor modified axially symmetric force-constant model. Both the dispersion curves and the force-constant model are qualitatively similar to those obtained for yttrium metal and yield long-range interactions in the basal plane, but interactions which decrease rapidly in the direction normal to the basal plane. A qualitative discussion is also given concerning the directional nature of the bonding in hcp metals from a consideration of the electron-phonon matrix elements. Evidence has been found for an anomaly along the Δ_1 branch reflecting the nesting feature of the Fermi surface along that direction. An unsuccessful search has been made for paramagnon-type excitations in this metal down to 4.2 K.

I. INTRODUCTION AND MEASUREMENTS

Scandium is the lightest element with an outer electronic configuration ($3d^1 4s^2$) similar to those of the rare-earth metals. Furthermore, energy-band calculations[1] have established that the conduction electron band structure and Fermi-surface geometry of scandium are very like those found for yttrium[2] ($4d^1 5s^2$) and the heavy rare-earth metals ($5d^1 6s^2$). The phonon spectra of this family of metals have recently been investigated by several groups. Studies of yttrium,[3] holmium,[4] and terbium[5] have already been reported. The measurements reported in this paper represent a continuation of the study of the phonon spectra of the rare-earth-type metals in order to investigate the extent to which the conduction electrons determine the structure of the dispersion curves.

Some relevant physical properties of scandium metals are listed in Table I. The crystal used had a volume of approximately 3.5 cc and was approximately cylindrical in shape. It was grown by a modified strain-anneal method.[6] It was tested for impurity concentrations of hydrogen, nitrogen, and oxygen by vacuum-fusion analysis from which the estimated impurity concentrations were as follows: H 7 ppm; N 71 ppm; and O 297 ppm by weight, respectively. The measurements were made at 295 K using the triple-axis neutron spectrometer at the Ames Laboratory Research Reactor. The apparatus has been described in Ref. 3. The "constant-Q" technique with fixed incident neutron energy was utilized. The incident energies used for different sets of runs were 50, 31, and 20 meV. The lower incident energies were used mainly to study the lower-frequency modes under high resolution and to investigate possible anomalies in the dispersion curves. Most of the measurements were made using the neutron-energy-loss process. The one-phonon peaks in the observed spectra were computer fitted and analyzed in a manner identical to that described in Ref. 3 and used to obtain points on the dispersion curves. Wherever possible, the one-phonon peaks corresponding to the transverse and some of the longitudinal branches were measured in the focused condition of the triple-axis spectrometer. Owing to the relatively large incoherent scattering cross section of scandium, some of the peaks corresponding to the relatively flat optical branches were con-

TABLE I. Physical properties of scandium.

Lattice constants[a]	$a = 3.309 \pm 2$ Å		$c = 5.268 \pm 7$ Å
Z	21		
Mass	44.956 amu		
Thermal neutron cross sections[b]			
Coherent	17.5 ± 1.5 b		
Incoherent	6.5 b		
Absorption	24.0 ± 1.0 b		
Elastic constants[c] (units of 10^{12} dyn/cm^2)		298 K	4 K
	c_{11}	0.993	1.032
	c_{33}	1.069	1.061
	c_{13}	0.294	•••
	c_{44}	0.277	0.272
	c_{66}	0.268	0.294

[a]K. A. Gschneidner, Jr., in *Transactions of the Vacuum Metallurgy Conference* (Am. Vac. Soc., Boston, Mass., 1966), p. 99.

[b]D. J. Hughes and R. B. Schwartz, *Neutron Cross Sections*, 2nd ed., (U.S. GPO, Washington, D. C., 1958).

[c]E. S. Fisher and D. Dever, in Proceedings of the Seventh Rare Earth Research Conference, 1968, Vol. 1, p. 237 (unpublished).

taminated by an incoherent inelastic peak in the scattered neutron intensity resulting from the high density of phonon states in this energy range, and hence the errors assigned to these branches are somewhat large. By and large, the dominant contribution to the error in a particular measured frequency was the statistical uncertainty in the peak position, as discussed in Ref. 3. In some cases, however, resolution effects played an important role in shifting the peak position, as will be discussed in Sec. IV with reference to the Δ_1 branch.

II. RESULTS

Measurements were made for the principal symmetry directions ΓA, ΓM, and ΓKM of the reciprocal lattice. Table II gives a list of the final set of measured phonon frequencies for these directions. Figure 1 shows a plot of the observed dispersion curves together with the predictions of the fitted-force-constant model discussed below. The relatively large scatter for the $\Sigma_3'(\mathrm{TO}_\perp)$ and $\Delta_2(\mathrm{LO})$ branches is due to the contamination by the incoherent inelastic peak referred to in Sec. I, and also due to poorer intensities for these higher-frequency modes. It is to be noted, that, as in yttrium,[3] there is a high degree of acoustic isotropy in the dispersion curves, as may also be seen in the measured elastic constants for scandium at room temperature (Table I). The initial slopes of the dispersion curves as given by the measured elastic constants are also indicated in Fig. 1, and it may be seen that except for the Δ_1 branch, the measured points are consistent with these slopes.

III. FORCE-CONSTANT MODEL AND DISCUSSION

As is well known, the low symmetry of the hexagonal close-packed structure leads, in the Born-von Karman phenomenology, to a large number of force constants within a relatively small number of neighbor distances. The use of the modified axially symmetric (MAS) force-constant model developed by DeWames *et al.*[7] helps considerably in reducing the number of independent force constants. However, there remains a further difficulty, in that even for the symmetry directions, the eigenfrequencies are in general rather complicated nonlinear functions of the force constants. In order to avoid the complexities of a nonlinear least-squares fitting procedure with its attendant uncertainties as to the position of the "best" minimum, therefore, a procedure based on obtaining a *linear* fit to the measured elastic constants and certain interplanar force constants obtained from the data was adopted.

The technique is essentially the same as that described in detail in Ref. 3. A Fourier analysis of the quantity $\omega^2(\vec{q})$ summed over all branches having the same irreducible representation along a particular direction yields "generalized interplanar force constants" which are linear combinations of the interatomic force constants. Other linear combinations may be obtained from the elastic constants C_{33}, $(C_{13}+C_{44})$, C_{44}, $(C_{11}-C_{66})$, and the expression for ω^2 at the symmetry point M. The appropriate linear relations are listed in the Appendix of Ref. 3. Finally, by using the above linear relations as well as solving directly for C_{11} alone, the MAS force constants may be obtained. The analysis revealed that at the very minimum, a sixth-neighbor MAS model was required to provide a reasonable representation of the dispersion curve. The sixth-neighbor MAS model provides an excellent fit for the ΓA direction, the ΓKM (T_2 and T_3) branches, and a reasonable fit for the ΓM branches, the biggest discrepancy being of the order of 10% for the

TABLE II. Phonon frequencies in scandium at 295 K.

$\vec{q}=(0,\ 0,\ \zeta)\times 2\pi/c$

Δ_1(LA)		Δ_2(LO)	
ζ	ν(THz)	ζ	ν(THz)
0.105	1.05 ± 0.02	0.0	6.91 ± 0.03
0.128	1.31 ± 0.02	0.05	6.89 ± 0.03
0.155	1.59 ± 0.02	0.1	6.83 ± 0.04
0.175	1.66 ± 0.03	0.12	6.69 ± 0.04
0.1875	1.94 ± 0.03	0.15	6.66 ± 0.04
0.2	1.98 ± 0.03	0.172	6.51 ± 0.03
0.2125	2.10 ± 0.02	0.2	6.58 ± 0.03
0.225	2.25 ± 0.01	0.257	6.29 ± 0.06
0.2375	2.29 ± 0.02	0.272	6.08 ± 0.03
0.25	2.38 ± 0.02	0.29	6.09 ± 0.02
0.2625	2.65 ± 0.02	0.3	6.01 ± 0.02
0.275	2.72 ± 0.02	0.34	5.78 ± 0.02
0.282	2.80 ± 0.02	0.39	5.50 ± 0.02
0.2875	2.84 ± 0.02	0.44	5.15 ± 0.05
0.293	2.95 ± 0.02	0.491	4.75 ± 0.02
0.3	2.97 ± 0.02		
0.3125	3.15 ± 0.02		
0.325	3.24 ± 0.02		
0.3375	3.34 ± 0.03		
0.35	3.43 ± 0.02		
0.375	3.69 ± 0.03		
0.3875	3.76 ± 0.04		
0.4	3.89 ± 0.04		
0.425	4.16 ± 0.02		
0.45	4.23 ± 0.02		
0.5	4.74 ± 0.03		

Δ_5(TA)		Δ_6(TO)	
ζ	ν(THz)	ζ	ν(THz)
0.1	0.62 ± 0.01	0.0	4.04 ± 0.04
0.15	0.89 ± 0.01	0.05	4.04 ± 0.07
0.2	1.17 ± 0.01	0.1	4.14 ± 0.04
0.25	1.47 ± 0.01	0.15	4.09 ± 0.04
0.3	1.83 ± 0.04	0.2	3.92 ± 0.04
0.35	2.05 ± 0.01	0.25	3.83 ± 0.05
0.41	2.38 ± 0.04	0.3	3.68 ± 0.04
0.5	2.87 ± 0.02	0.35	3.51 ± 0.03
		0.4	3.35 ± 0.02

TABLE II. (*Continued*)

$\vec{q} = (\zeta, 0, 0) \times 4\pi/\sqrt{3}a$

Σ_1(LA) ζ	ν(THz)	Σ_1(LO) ζ	ν(THz)
0.09	1.75 ± 0.02	0.0	4.04 ± 0.04
0.1	2.00 ± 0.02	0.05	4.08 ± 0.04
0.125	2.43 ± 0.01	0.1	4.41 ± 0.03
0.15	2.86 ± 0.01	0.15	4.71 ± 0.03
0.175	3.37 ± 0.02	0.2	5.22 ± 0.02
0.2	3.77 ± 0.02	0.25	5.66 ± 0.02
0.225	4.20 ± 0.02	0.3	5.93 ± 0.04
0.25	4.52 ± 0.02	0.35	5.92 ± 0.04
0.275	4.87 ± 0.01	0.4	6.05 ± 0.02
0.3	5.22 ± 0.02	0.5	6.23 ± 0.05
0.35	5.70 ± 0.02		
0.5	6.21 ± 0.1		

Σ_3(TA$_\perp$) ζ	ν(THz)	Σ_3(TO$_\perp$) ζ	ν(THz)
0.1	1.07 ± 0.01	0.0	6.91 ± 0.03
0.15	1.59 ± 0.01	0.05	6.70 ± 0.03
0.2	2.10 ± 0.01	0.1	6.58 ± 0.06
0.3	3.06 ± 0.02	0.2	6.59 ± 0.06
0.4	3.75 ± 0.02	0.25	6.51 ± 0.03
0.45	4.08 ± 0.03	0.3	6.38 ± 0.05
0.5	3.97 ± 0.02	0.4	6.39 ± 0.04
		0.45	6.11 ± 0.06
		0.5	6.23 ± 0.04

Σ_4(TA$_\parallel$) ζ	ν(THz)	Σ_4(TO$_\parallel$) ζ	ν(THz)
0.15	1.60 ± 0.01	0.0	4.04 ± 0.04
0.2	2.12 ± 0.01	0.05	4.11 ± 0.03
0.25	2.58 ± 0.01	0.1	4.30 ± 0.03
0.3	2.96 ± 0.01	0.15	4.55 ± 0.03
0.35	3.30 ± 0.03	0.2	4.88 ± 0.03
0.4	3.49 ± 0.03	0.25	5.15 ± 0.04
0.45	3.69 ± 0.04	0.3	5.49 ± 0.02
0.5	3.57 ± 0.04	0.35	5.66 ± 0.03
		0.4	5.90 ± 0.02
		0.5	6.11 ± 0.04

$\vec{q} = (\zeta, \zeta, 0) \times 4\pi/a$

T_3(TA$_\perp$) ζ	ν(THz)	T_2(TO$_\perp$) ζ	ν(THz)
0.1	1.83 ± 0.01	0.0	6.91 ± 0.03
0.15	2.79 ± 0.01	0.05	6.87 ± 0.05
0.2	3.61 ± 0.01	0.1	6.85 ± 0.05
0.25	4.32 ± 0.02	0.2	6.41 ± 0.04
0.3	5.00 ± 0.02	0.25	6.08 ± 0.05
0.4	5.86 ± 0.02	0.3	5.67 ± 0.03
0.45	6.16 ± 0.07	0.333	5.35 ± 0.03
0.5	6.23 ± 0.04	0.4	4.68 ± 0.06
		0.45	4.19 ± 0.04
		0.5	3.97 ± 0.02

TA$^{\parallel}$(Σ_4) branch in that direction. The dispersion curves according to this model are shown in Fig. 1. The force constants so determined are listed in Table III, where they are expressed in both MAS and general tensor form according to the notation of Czachor.[8] Using this model, and the program HCPGNU developed by Rauberheimer and Gilat[9] the frequency distribution function $g(\nu)$ was calculated and is illustrated in Fig. 2, where some of the critical points associated with symmetry direction points are also indicated. Figure 3 shows the Debye temperature calculated from $g(\nu)$ as a function of temperature. Also shown are the values obtained experimentally by Flotow and Osborne.[10] The agreement is reasonable in view of the combined uncertainties in the harmonic approximation using the room-temperature force-constant model and the uncertainties in the experimental values. The force-constant model was also used to calculate the Debye-Waller factor for scandium. This may be written as

$$e^{-2W} = \exp\{-(\hbar^2/2M)[(K_\parallel^2/k_B\Theta_0)G_\parallel(T/\Theta_0) + (K_\perp^2/k_B\Theta_0)G_\perp(T/\Theta_0)]\}\ , \quad (1)$$

where M is the atomic mass, $(\hbar K_\parallel)$ and $(\hbar K_\perp)$ are, respectively, the components of momentum transfer parallel and perpendicular to the basal plane, and Θ_0 is some reference Debye temperature which is taken to be Θ at 0 K. For all hcp metals whose phonon frequencies scale in the ratio of their Θ_0's, $G_\parallel$ and $G_\perp$ may be taken to be universal dimensionless functions of (T/Θ_0). The functions $G_\parallel$ and $G_\perp$ for Sc are tabulated in Table IV.

The contribution to the dynamical matrix may be split up into an electrostatic interaction between the ion cores, the ion-ion interaction via the conduction electrons, and finally the direct ion-core "overlap" interaction. For hexagonal metals having identical numbers of conduction electrons per atom and similar conduction electron energy bands, it may be shown quite generally that the sum of the first two contributions to the dynamical matrix scale approximately in the ratio of the respective squares of their ion-plasma frequencies given by $\omega_p^2 = 4\pi Ne^2/M$, where N is the number of ions per unit volume and M is the ionic mass. Therefore in the small-core approximation, one might expect yttrium and scandium to have frequencies which scale in the ratio of their ω_p's. Indeed the measured dispersion curves do look remarkably similar and Table V lists ω/ω_p for both metals for selected points in the zone. It may be seen that they are within 10% of each other. A similar detailed comparison with the phonon frequencies of the heavy rare-earth metals has not yet been made but would be interesting in order to examine the possible influence of the $4f$ shells on the dispersion curves.

The frequency distribution function and the Debye-Waller functions $G_\parallel$ and $G_\perp$ of scandium also look similar to those obtained for yttrium, the maximum

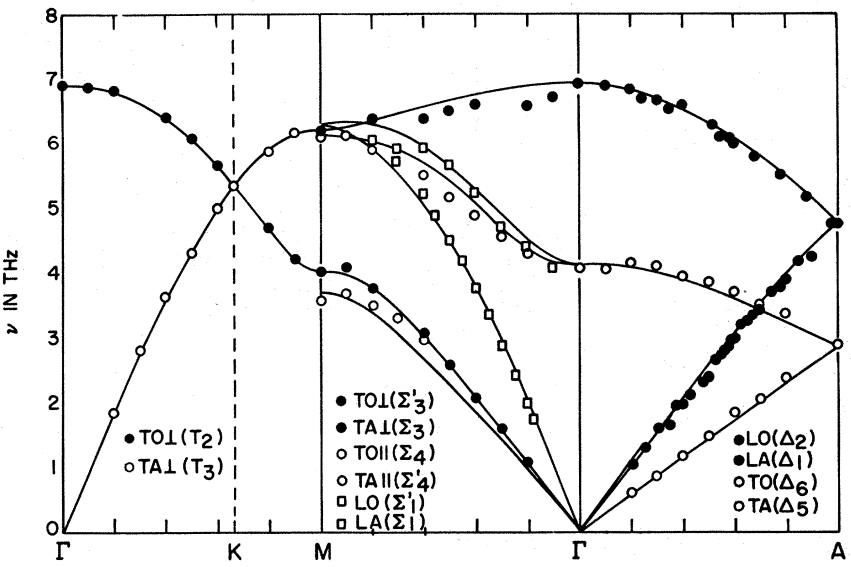

FIG. 1. Phonon dispersion curves for symmetry directions in scandium at room temperature. The smooth curves represent the sixth-neighbor MAS-model fit.

discrepancy being about 16% at $T/\Theta_0 = 2$.

As in the case of yttrium, the interaction between the origin atom and the fourth neighbor located at $(0, 0, c)$ is small compared to the interaction with the fifth and sixth neighbors located, respectively, in the basal plane and the layers adjacent to the basal plane. This also manifests itself in the fact that $\omega^2(\vec{q})$ along the c axis for both longitudinal and transverse branches is dominated in each case by only one interplanar force constant. If we suppose a linear-combination-of-atomic orbitals (LCAO) approximation is used to represent wave functions of the conduction electrons in metallic scandium, then these LCAO's may be regarded as made up of s and d orbitals. The d orbitals in a crystalline field of hexagonal symmetry may be classified as A_{1g}, E_{1g}, and E_{2g} where A_{1g} has lobes directed along the c axis, whereas the others possess a node in this direction. If the wave functions of the occupied states of the conduction band are principally of the E_{1g} and E_{2g} type, then the bonding by means of such orbitals will be very small between atoms separated along the c axis, as seems to be the case for Sc and Y. The symmetry properties of the occupied states of the conduction bands of a rare-earth-type metal have been classified at the principal symmetry points of the Brillouin zone by Dimmock, Freeman, and Watson.[11] Their calculation is actually for gadolinium. However, as mentioned in the introduction, because of the similarity of their conduction bands, the symmetry properties of the occupied conduction-band states of Sc can be inferred from those of Gd. Examination of these symmetry classifications shows that the A_{1g}-type orbital can only be appreciably mixed into the occupied conduction-state wave functions for the doubly degenerate level (K_5) near K, for the doubly degenerate level (A_1) near A, and possibly for the levels (M_1, M_2) near M. The above arguments suggest that in fact the over-all projection of A_{1g}-type orbitals in the occupied density of states is rather small for these metals. On the other hand, zirconium, which has one more conduction electron per atom, has a very flat LO branch along the c axis, suggesting strong interaction between the origin atom and its neighbors out along the c axis.[12] In this connection, it is perhaps significant that the calculations of Loucks[13]

TABLE III. Force constants for the sixth-neighbor MAS model. Units are in dyn/cm.

Neighbor	GTF notation	MAS notation
1	$A_1 = 3421.2$	$\delta_1 = 1999.2$
	$B_1 = -577.2$	$\epsilon_{1x} = -2576.4$
	$G_1 = 12641.0$	$\epsilon_{1z} = -2559.9$
2	$a_1 = 5322.5$	$\alpha_2 = 11793.0$
	$b_1 = 11219.0$	$\beta_{2x} = 2374.2$
	$g_1 = 1525.1$	$\beta_{2z} = 1525.1$
3	$A_2 = 2284.0$	$\delta_3 = -421.3$
	$B_2 = -4457.5$	$\epsilon_{3x} = 2284.0$
	$G_2 = -1222.3$	$\epsilon_{3z} = 1981.1$
4	$a_2 = -622.7$	$\beta_{4x} = -622.7$
	$g_2 = -609.7$	$\alpha_4 + \beta_{4z} = -609.7$
5	$A_3 = 1738.6$	$\delta_5 = 99.9$
	$B_3 = 2138.4$	$\epsilon_{5x} = 539.2$
	$G_3 = 111.5$	$\epsilon_{5z} = -648.1$
6	$a_3 = -40.5$	$\alpha_6 = 1307.3$
	$b_3 = 1266.8$	$\beta_{6x} = -40.5$
	$g_3 = -114.7$	$\beta_{6z} = -114.7$

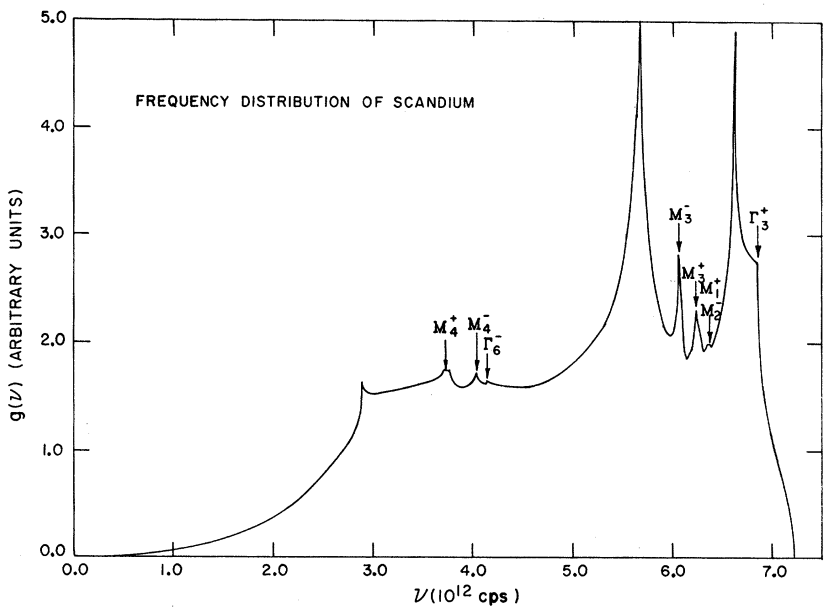

FIG. 2. Frequency spectrum $g(\nu)$ for scandium showing critical points arising from symmetry directions only.

show that in zirconium, the principal bands along the symmetry directions which become occupied compared to the rare-earth metals are the doubly degenerate bands connecting the levels H_2 and A_1 which are allowed near A to mix in A_{1g}-type orbitals in their wave functions, and the bands of symmetry T_1' along KM and U_1 along LM, each of which can also contain appreciable A_{1g}-type orbitals. Thus, it would seem likely that the addition of an extra electron appreciably increases the projection of A_{1g}-type orbitals in the occupied states and hence significantly increases bonding along the c axis.

IV. FERMI-SURFACE EFFECTS

The magnetic properties of several scandium–rare-earth alloys have been studied by neutron diffraction[14,15] and for a certain minimum concentration of a rare earth in scandium (about 25% in the case of Tb in Sc) a spiral spin configuration has been observed at low temperatures where, of course, it is only the moments on the rare-earth atoms which order. For sufficiently dilute rare-earth concentrations the ordering corresponds to a spiral along the c axis with the magnetic ordering wave vector $\vec{q}_m$ converging to a value of $(0, 0, 0.28)\times 2\pi/c$. As is well known, the magnetic structure is determined by a wave vector $\vec{q}_m$ for which the wave-number-dependent generalized susceptibility function in the paramagnetic phase, $\chi^{(0)}(\vec{q})$, has a maximum. Since, for reasons discussed previously, the dilute

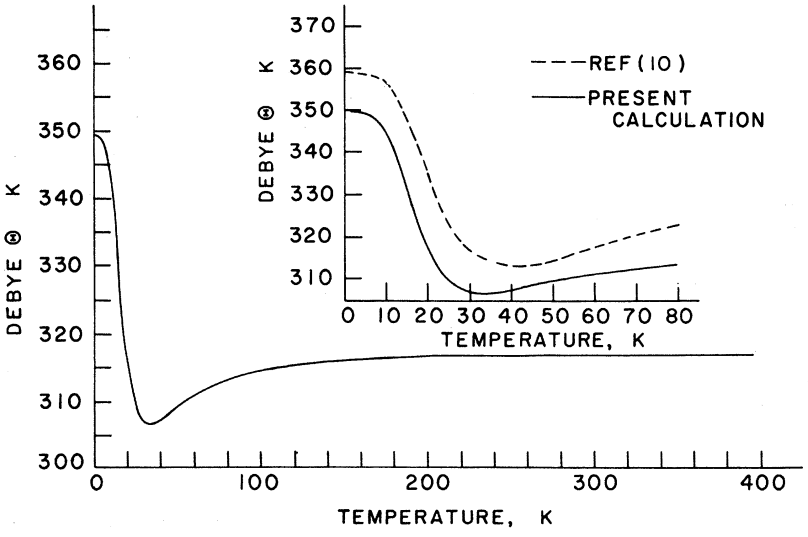

FIG. 3. Plot of Debye temperature vs T calculated from $g(\nu)$ shown in Fig. 2. Inset shows a comparison with the experimental results of Flotow and Osborne (Ref. 10).

TABLE IV. The dimensionless functions $G_{\parallel}(T/\Theta_0)$ and $G_{\perp}(T/\Theta_0)$ appearing in Eq. (1) for the Debye-Waller factor.

T/Θ_0	$G_{\parallel}(T/\Theta_0)$	$G_{\perp}(T/\Theta_0)$
0.05	1.686	1.752
0.10	3.460	3.599
0.15	5.386_5	5.618
0.20	7.521	7.869
0.25	9.901_5	10.395
0.30	12.557	13.224
0.35	15.505	16.371
0.40	18.740	19.830
0.45	22.286	23.636
0.50	26.157	27.795
0.6	34.892	37.191
0.7	44.977	48.052
0.8	56.432	60.397
0.9	69.269	74.241
1.0	83.498	89.592
1.2	116.16	124.84
1.4	154.45	166.18
1.6	198.40	213.64
1.8	248.01	266.90
1.95	287.96	309.88

alloys have $\vec{q}_m = (0, 0, 0.28) \times 2\pi/c$, this seems to indicate that $\chi^{(0)}(\vec{q})$ of pure scandium has a maximum around this wave vector. Further, the diagonal element of the dielectric function $\epsilon(\vec{q}, \vec{q})$ is related to $\chi^{(0)}(\vec{q})$ by the relation

$$\epsilon(\vec{q}, \vec{q}) = 1 + Av(\vec{q})\chi^{(0)}(\vec{q}), \tag{2}$$

where A is a constant and $v(\vec{q})$ is the transform of the electrostatic electron-electron interaction including exchange and correlation effects. Since the dielectric screening by the conduction electrons plays a key role in determining the ion-ion interaction transmitted by the conduction electrons, one might expect a sharp maximum in $\chi^{(0)}(\vec{q})$ to manifest itself also as an anomaly in the dispersion curves. In fact, it may be shown that one would expect a sharp dip in the longitudinal acoustic branch at a $\vec{q} = (0, 0, 0.28) \times 2\pi/c$.

A careful search was made for such anomalies in the Δ_1 branch, which included doing several scans along this branch under varied experimental conditions and at rather closely spaced values of the wave vector along this branch. Four sets of runs were made using incident energies of 20, 50, 31, and 31 meV, respectively. The first was run with neutron energy gain and the other three with neutron energy loss. The first three were run from the (004) lattice point in a purely longitudinal configuration ($\vec{Q} \parallel \vec{q}$) and the last set was run from the $(\bar{1}, \bar{1}, 2)$ lattice point, thus taking advantage of the partial focusing provided by some transverse component of $\vec{q}$.[3] The best resolution was achieved for the last set, i.e., for the partially focused energy-loss neutron groups around the $(\bar{1}, \bar{1}, 2)$ lattice point with an E_0 of 31 meV. This scan is shown in Fig. 4, where it may be seen that there does seem to be a dip in the dispersion curve between $\vec{q} = (0, 0, 0.2) \times 2\pi/c$ and $\vec{q} = (0, 0, 0.3) \times 2\pi/c$. The same effect was in fact seen in each of the above scans. However, the different sets of runs had small systematic discrepancies between each other (due perhaps to systematic instrumental errors or to the effects of finite instrumental resolution) so that the over-all scatter of all measured points for that branch is at least equal to the size of the effect. Nevertheless, for each individual set of measured points, the effect was significant compared to the scatter of points on that branch, so that the dip, though small in magnitude, is probably real. Further evidence for this was provided by the fact that in the region between $(0, 0, 0.25) \times 2\pi/c$ and $(0, 0, 0.35) \times 2\pi/c$ the peak shapes of the scattered neutron groups displayed a broad and asymmetric shape. If we represent the dip as a joining of two parts of the dispersion curve with different slope, the anomalous peak shapes may be understood in terms of the resolution ellipsoid[16] cutting through the dispersion surface at different wave vectors relative to this intersection point in the course of a constant-Q scan parallel to the E axis. In such cases the two regions of different slope will give rise to maximum intensity at different E values, resulting in an asymmetric or even double-humped peak. In order to test this hypothesis, the instrumental resolution function for the spectrometer was estimated using the theory of Cooper and Nathans.[16] It was verified that this function gave the widths of various scans across a number of Bragg reflections correctly. It was then calculated for the energy transfers involved for the phonons in the vicinity of the anomaly. This was then numerically folded along the E axis with

TABLE V. (ν/ν_p) of scandium and yttrium for some symmetry points.

	$(\nu/\nu_p)_{\text{scandium}}$	$(\nu/\nu_p)_{\text{yttrium}}$
Γ_6^-	0.215	0.230
Γ_3^+	0.367	0.398
A_1	0.252	0.275
A_2	0.158	0.168
$M_1^+(\text{LA})$	0.330	0.345
$M_3^+(\text{TO}_\perp)$	0.331	0.355
$M_4^+(\text{TA}_\parallel)$	0.190	0.197
$M_3^-(\text{TO}_\parallel)$	0.324	0.347
$M_4^-(\text{TA}_\perp)$	0.211	0.229
K_6	0.284	0.294

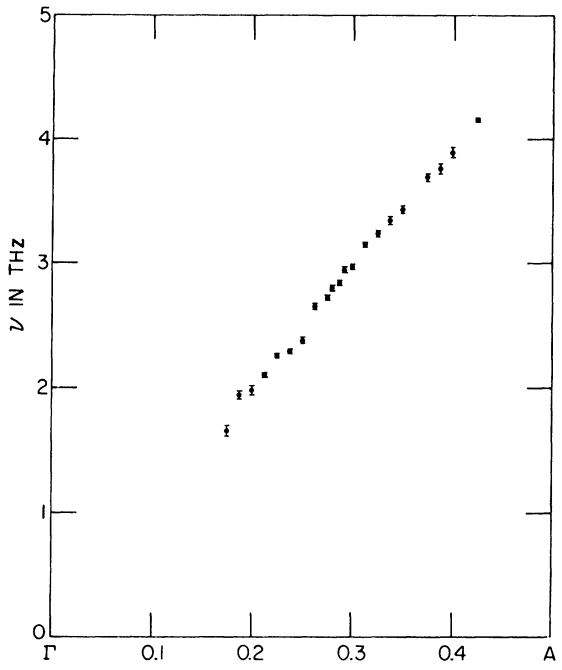

FIG. 4. The Δ_1 branch for scandium measured with $E_0 = 31$ meV from the $(\bar{1}, \bar{1}, 2)$ reciprocal-lattice point. The error bars represent only the statistical uncertainty in the peak positions of the neutron groups.

a dispersion surface represented by two semi-infinite planes with different slopes c_1 and c_2 intersecting at $(0, 0, \zeta)\times 2\pi/c$. If c_1 and c_2 were chosen as 7.5 and 9.0 THz Å, respectively, and ζ was chosen as 0.27, it was found that good agreement was obtained for almost all the peaks obtained for the Δ_1 branch in this region, including the sets of runs with quite different instrumental conditions. Figure 5 shows the computed and observed line shapes for some of the peaks in the anomaly region for the highest-resolution set of runs shown in Fig. 4. One may observe how the asymmetry reverses itself as the wave vector in question goes from one side of the anomaly to the other. It is to be noted that neither of the peaks in the double-peak structure has a position corresponding exactly to the value of the actual frequency for the set wave vector. Further, the effect of taking the mean of the scattered neutron group, as was conventionally done in this analysis, is to smooth the effect of the dip but not to remove it entirely. To summarize, an analysis in terms of the resolution function confirms that our observations on the Δ_1 branch are consistent with a dip or anomalous change of slope at $\vec{q} = (0, 0, 0.27)\times 2\pi/c$ which is remarkably close to the value for the peak in $\chi^{(0)}(\vec{q})$ for Sc estimated from the magnetic-structure data.

The peak in $\chi^{(0)}(\vec{q})$ probably arises from a "nesting" feature of the Fermi surface in scandium along the c axis as has been pointed out by several authors.[17,18] The energy-band calculations of Fleming and Loucks[1] were used together with the programs devised by Liu *et al.*[19] to evaluate $\chi^{(0)}(\vec{q})$ using the approximation for the (unenhanced) susceptibility function,

$$\chi^{(0)}(\vec{q}) = \sum_{k,b,b} \frac{n(\vec{k}, b) - n(\vec{k}+\vec{q}, b')}{E(\vec{k}, b) - E(\vec{k}+\vec{q}, b')}, \tag{3}$$

where $n(\vec{k},b)$ denotes the occupation number for the state with Bloch wave vector $\vec{k}$ and band index b, and $E(\vec{k},b)$ is the appropriate energy. Only the 3rd and 4th bands (which determine the Fermi surface) were used in the calculation. The resultant $\chi^{(0)}(\vec{q})$ exhibits a peak at $\vec{q} = (0, 0, 0.35)\times 2\pi/c$, which we believe corresponds to the one found experimentally. The effect of including matrix elements in Eq. (4) would probably be to pull the peak in to a smaller $\vec{q}$ value. Another peak was found in the calculation at $\vec{q} = (0, 0, 0.8)\times 2\pi/c$, which would presumably produce an effect on the optical (Δ_2) branch along ΓA. Unfortunately, the poorer quality of the data for this branch (for reasons given in Sec. II) precluded any search for an anomaly in this branch. It is interesting to note that in yttrium some evidence was found for small anomalies on the Δ_2 branch but none was found on the Δ_1

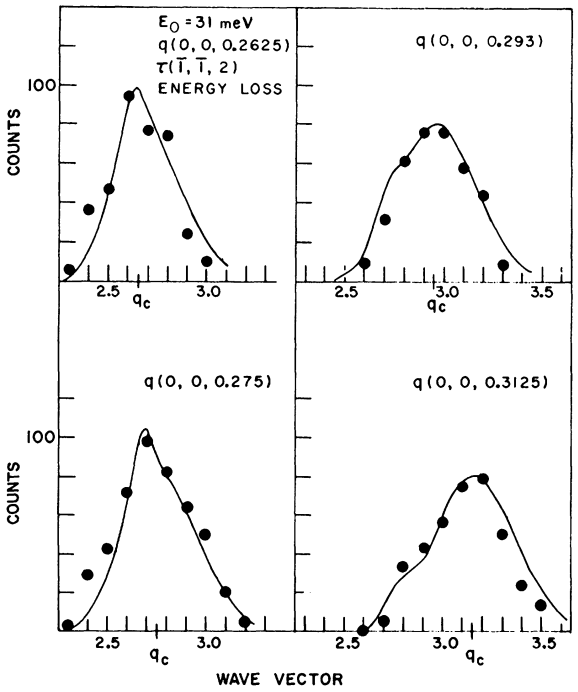

FIG. 5. Neutron groups observed in the region of the anomaly on the Δ_1 branch together with peak shapes calculated using the instrumental resolution function in the manner described in the text.

branch.

Finally, we describe a search for spontaneous antiferromagnetic spin fluctuations among the conduction electrons of scandium. It is known that in very dilute alloys of Gd in Sc, the Gd^{3+} ions exhibit considerable moment enhancement over their free-ion value, possibly owing to the exchange enhancement of the generalized susceptibility function $\chi^{(0)}(\vec{q})$ for the noninteracting conduction electrons. The relatively high density of states for scandium at the Fermi level and the assumed peak in $\chi^{(0)}(\vec{q})$ result in a large exchange-enhancement factor $[1-v\chi^{(0)}(\vec{q})]^{-1}$ (where v is the exchange interaction between conduction electrons) for $\vec{q}$ in the region of this peak, resulting in antiferromagnetic correlations transmitted via the conduction electrons, which would explain the peculiar field dependence of dilute Gd-Sc alloys.[20] Ferromagnetic coupling of the conduction electron polarization to the impurity spin would also explain the giant moment.[21] It has further been suggested that the smallness of the dynamic exchange-enhancement denominator $[1-v\chi^{(0)}(\vec{q},\omega)]$ for certain values for $\vec{q}$ close to the "nesting" $\vec{q}$ would lead to spontaneous antiferromagnetic spin fluctuations or paramagnonlike excitations among the conduction electrons[22] even though a static moment may not exist. Such excitations have, in fact, been recently observed by neutron scattering in the case of paramagnetic Cr-Mn alloys,[23] which in principle provides an example of a closely related system. Accordingly, a search was made for peaks in the inelastically scattered neutron energy spectrum in the neighborhood of $\vec{q}=(0,0,0.27)\times 2\pi/c$ which could be ascribed to this effect. Scans were made in both the "constant-Q" and "constant-E" modes, and also both at room temperature and 4.2 K. The only significant peak which was observed was a small one which occurred at the frequency of the transverse optic (Δ_6) phonon branch for this wave vector. Although this process is normally forbidden for the conditions under which the scans were done (where $\vec{Q}$ was always parallel to $\vec{q}$), we ascribed its appearance to a combined one-phonon–Bragg-scattering process. In any case, it did not change intensity or width at all significantly between 295 and 4.2 K, as opposed to the behavior expected of paramagnons.[24] We conclude, therefore, that the paramagnons in scandium are either extremely broad or have quite low neutron scattering cross sections. This would imply that the generalized exchange-enhanced susceptibility of scandium

$$\chi(\vec{q},\omega)=\frac{\chi^{(0)}(\vec{q},\omega)}{1-v\chi^{(0)}(\vec{q},\omega)}$$

[where $\chi^{(0)}(\vec{q},\omega)$ is the unenhanced susceptibility] does not have any appreciable poles close to the real ω axis.

ACKNOWLEDGMENTS

The authors would like to thank B. Beaudry for growing the single-crystal scandium sample, Dr. T. O. Brun for the use of his computer programs and for helpful advice, Dr. S. H. Liu, Dr. T. L. Loucks, and Dr. R. P. Gupta for helpful discussions regarding the Fermi-surface and paramagnon effects, and Dr. J. O. Dimmock and Dr. L. Hodges for valuable comments relating to the symmetries of the wave functions of the rare-earth metals.

---

†Work performed in the Ames Laboratory of the U. S. Atomic Energy Commission, Contribution No. 2996 (unpublished).

*Present address: Solid State Division, Oak Ridge National Laboratory, Oak Ridge, Tenn. 37830.

[1]G. S. Fleming and T. L. Loucks, Phys. Rev. 173, 685 (1968).

[2]T. L. Loucks, Phys. Rev. 144, 504 (1966).

[3]S. K. Sinha, T. O. Brun, L. D. Muhlestein, and J. Sakurai, Phys. Rev. B 1, 2430 (1970).

[4]J. A. Leake, V. J. Minciewicz, and G. Shirane, Solid State Commun. 7, 535 (1969); R. M. Nicklow, N. Wakabayashi, and P. R. Vijayaraghavan, Phys. Rev. B 4, 1229 (1971).

[5]J. C. Gylden Houman and R. M. Nicklow, Phys. Rev. B 1, 3943 (1970).

[6]B. J. Beaudry (private communication). The crystal was grown using a modification of the method described by Nigh [H. E. Nigh, J. Appl. Phys. 34, 3323 (1963)].

[7]R. E. DeWames, T. Wolfram, and G. W. Lehman, Phys. Rev. 138, A717 (1965).

[8]A. Czachor, in *Proceedings of the Bombay Symposium on Inelastic Scattering of Neutrons in Solids and Liquids* (International Atomic Energy Agency, Vienna, 1965), Vol. 1, p. 181.

[9]L. J. Raubenheimer and G. Gilat, Phys. Rev. 157, 586 (1967).

[10]H. E. Flotow and D. W. Osborne, Phys. Rev. 160, 467 (1967).

[11]J. O. Dimmock, A. J. Freeman, and R. E. Watson, in *Optical Properties and Electronic Structure of Metals and Alloys* (North-Holland, Amsterdam, 1966), p. 237.

[12]H. F. Bezdek, R. E. Schmunk, and L. Finegold, Phys. Status Solidi 42, 275 (1970).

[13]T. L. Loucks, Phys. Rev. 159, 544 (1967).

[14]H. R. Child and W. C. Koehler, J. Appl. Phys. 37, 1353 (1966).

[15]H. R. Child and W. C. Koehler, Phys. Rev. 174, 562 (1968).

[16]M. J. Cooper and R. Nathans, Acta Cryst. 23, 357 (1967).

[17]S. C. Keeton and T. L. Loucks, Phys. Rev. 168, 672 (1968).

[18]W. E. Evenson and S. H. Liu, Phys. Rev. 178, 783 (1969).

[19]S. H. Liu, R. P. Gupta, and S. K. Sinha, Phys. Rev. B (to be published).

[20]F. Y. Fradin, J. W. Ross, L. L. Isaacs, and D. J.

Lam, Phys. Letters 28A, 276 (1968).
[21]D. K. Wohlleben, Phys. Rev. Letters 21, 1343 (1968).
[22]T. L. Loucks (private communication).
[23]S. K. Sinha, S. H. Liu, L. D. Muhlestein, and N. Wakabayashi, Phys. Rev. Letters 23, 311 (1969).
[24]S. H. Liu, Phys. Rev. B 7, 2664 (1970).

PHYSICAL REVIEW B VOLUME 4, NUMBER 8 15 OCTOBER 1971

Binding Energies of Transition-Metal Atoms Adsorbed on a Transition Metal

F. Cyrot-Lackmann
Institut Laue - Langevin, Cedex 156, 38 - *Grenoble-Gare, France*

and

F. Ducastelle
Office National d'Etudes et de Recherches Aerospatiales, 92 - *Chatillon, France*

(Received 16 February 1971)

The binding energies of transition-metal atoms of the 5*d* series adsorbed on a 5*d* transition metal are calculated in the tight-binding approximation. The general features of the variation of the binding energy with the number of adatom 5*d* electrons are similar for all the substrates. It shows a parabolic behavior with a maximum of the order of the cohesive energy for the substrate, and a subsequent sharper decrease as the number of adatom 5*d* electrons is increased. The maximum is always located close to tungsten, as in the case of a tungsten substrate, where it is between tungsten and rhenium.

Some measurements have been made recently of the binding energy[1] and diffusion[2] of third-transition-series metals on various single crystal planes of tungsten, using a field ion microscope technique. The binding energies were deduced from field-desorption data and are subject to some uncertainty in their quantitative determination.[3] However the rise in the adatom binding energy to a maximum for rhenium, similar to the maximum in the cohesive energies for 5*d* transition metals, and the subsequent sharper decrease as the number of adatom 5*d* electrons is increased seem now well established (Fig. 1).

Several attempts at attaining a theoretical understanding of the binding energy have already been made, based either on a tight-binding model,[4,5] or on a virtual-bound-state model.[6] Recently, Newns has also discussed the importance of correlation in this problem.[7]

It seems more reasonable to study the binding energy of transition-metal atoms on a transition metal, by using a tight-binding approach, as the tight-binding *d*-band-broadening contribution to the cohesive energy of transition metals dominates for the majority of transition metals.[8,9]

Here, we will calculate the binding energies of the 5*d* transition-series atoms on a 5*d* transition metal, using a tight-binding model, taking into account somewhat more realistically some parameters, such as the real crystalline structure of the substrate and the degeneracy of the *d* band. But consequently, we are only able to take into account self-consistency in a phenomenological way, and our results are particularly valid for adatoms having approximately the same number of *d* electrons as the substrate.

We use a moments technique, already used with some fair success to describe various properties of transition metals.[4,8,10] The method and the approximations have already been described elsewhere.[4,10] Let us just recall that we are using a Hartree scheme with a tight-binding description of the *d* band, neglecting the contribution of the *s* band and of *s*-*d* mixing. As usual, we use a two-center approximation involving two kinds of overlap integrals, the crystalline ones α, and the transfer type β, involved, respectively, in the shift of the *d* band and its width. The overlap integrals α and β are strictly defined as 5×5 matrices[10] but, in fact, due to the smallness of the crystalline ones, one can take an average value α equal to the shift of the band for them. On the other hand, following the notations of Slater and Koster,[11] and from the second moment, one can define the square of an effective overlap integral β^2 as $5\beta^2 = dd\sigma^2 + 2dd\pi^2 + 2dd\delta^2$. β^2 is also directly related to the width of the *d* band.[10]

One starts from a perfect transition-metal M surface and a free transition atom A, and then the atom A is absorbed on the surface of M, the coupling between them being established through the overlap integrals. The binding energy $U_B(A-M)$ of the adatom A can then be defined as the difference between the total energy before and after the atom A had been absorbed on M. Clearly the expression of $U_B(A-M)$ will involve the variation of geometry of the sys-